PERGAMON

International Journal of Solids and Structures 37 (2000) 6891–6915

INTERNATIONAL JOURNAL OF SOLIDS and STRUCTURES

www.elsevier.com/locate/ijsolstr

The effect of imperfect boundary conditions on the collapse behavior of anisotropic shells

J. Arbocz *

Delft University of Technology, Koiter Institute, Postbus 5058, 2600 Delft, Netherlands

Received 10 November 1999

Abstract

A rigorous solution is presented for the case of stiffened anisotropic shells with general imperfections under combined axial compression, internal or external pressure and torsion. Donnell type equations are used to describe the behavior of the layered composite shell. The stiffeners are represented by smeared theory and for the discrete end rings, Cohen's ring equations are used. The circumferential dependence is eliminated by a truncated Fourier series. The resulting 2-point boundary value problem is solved numerically via the "parallel shooting method".

The nonlinear collapse behavior is studied using different combinations of axisymmetric and asymmetric imperfections. Comparison with Koiter type imperfection predictions display the range of validity of the asymptotic results.

It is shown that besides initial geometric imperfections also nonuniform harmonically varying boundary conditions can have severe degrading effect on the load carrying capacity of anisotropic shells.

Keywords: Boundary conditions; Collapse behavior; Anisotropic shells

1. Introduction

The use of large general-purpose computer programs for the analysis of different types of structures is by now well accepted. These codes have been used successfully to calculate the stress distributions and deformation patterns for very complicated structural configurations with the accuracy demanded in engineering applications under all kind of loading conditions. However, if the structure is buckling sensitive, then even, in 1998, one will often encounter great difficulties in making an accurate and reliable prediction of the critical buckling load.

The perplexing behavior of axially compressed thin-walled cylindrical shells has been a major concern for structural engineers for over 75 years and it represents one of the best known examples of the very complicated stability behavior which can occur with thin-walled structures. The whole problem is well illustrated in Fig. 1 (Weller and Singer, 1971), where some of the available experimental results for axially compressed stringer stiffened shells are plotted as a function of Batdorf's $Z(=L^2/Rt\sqrt{1-\nu^2})$ parameter.

* Corresponding author.
E-mail address: j.arbocz@lr.tudelft.nl (J. Arbocz).

0020-7683/00/$ - see front matter
PII: S0020-7683(99)00319-4

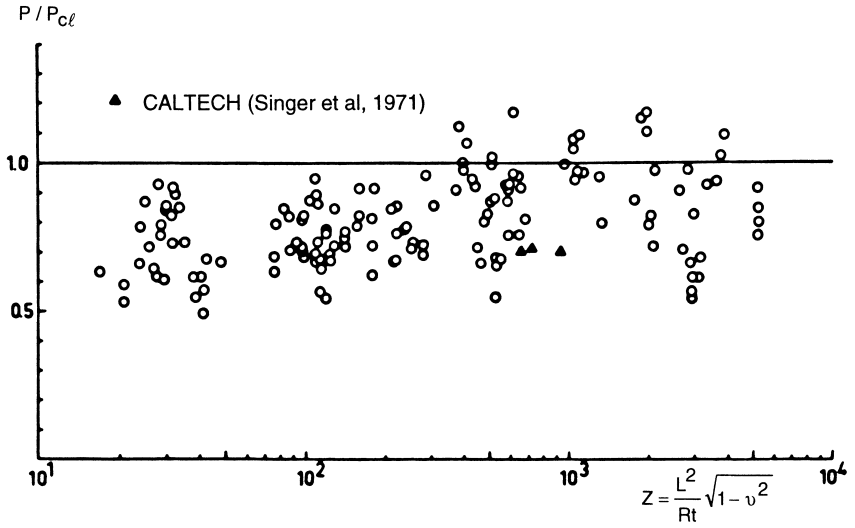

Fig. 1. Comparison of theory and experiment for stringer stiffened shells (Weller and Singer, 1971).

Notice that the experimental buckling loads are normalized by the "classical" linear buckling loads, computed using membrane prebuckling and SS-3 ($N_x = v = w = M_x = 0$) boundary conditions.

Trying to find an explanation for the wide experimental scatter and for the poor correlation between the theoretical predictions based on a linearized small deflection theory with SS-3 boundary conditions and the experimental results has occupied some of the most eminent scientists of this century. Thanks to the pioneering work by Koiter (1945, 1967, 1963) and the Harvard group under Budiansky and Hutchinson (1964), Budiansky (1965) and Hutchinson and Amazigo (1967) initial geometric imperfections have been accepted as one of the principal factors causing the wide scatter of experimental buckling loads shown in Fig. 1. In addition, Hoff (1961) and Ohira (1961) using membrane prebuckling analysis have shown that for isotropic shells different in-plane boundary conditions can also cause large variations in the critical buckling loads. Thus, for instance, for the so-called weak boundary condition where no tangential stresses are exerted on the ends of the shell, they found that the classical buckling load is reduced by a factor of two. Almroth (1965) using a rigorous nonlinear prebuckling analysis essentially confirmed these results. In a later paper, Hoff and Soong (1969) showed that for isotropic shells relaxing the tangential restraint along a small fraction of the edge has an almost equally detrimental effect. Recently, Singer (1979, 1983) have developed an experimental vibration correlation technique, which makes it possible to estimate the degree of elastic support present in a particular test setup.

Despite all these theoretical and experimental results the shell design manuals in use at the present time (Anonymous, 1968, 1988) adhere to the so-called "lower bound design philosophy" and as such recommend the use of the following buckling formula:

$$P_a \leqslant \frac{\gamma}{FS} P_c, \tag{1}$$

where P_a is the allowable applied load, P_c is the critical buckling load of the perfect structure, γ is the so-called "knockdown factor" and FS is a factor of safety. The empirical knockdown factor, γ is so chosen that when it is multiplied with the critical buckling load of the perfect structure a "lower bound" to all existing experimental data are obtained.

It has long been felt that while for many cases the lower bound design philosophy provides a safe and reliable buckling load prediction, it penalizes innovative shell designs because of the poor experimental

results obtained with shells produced and tested under completely different circumstances. It has been hoped that with the large scale introduction of computer codes with advanced nonlinear capabilities an alternate design procedure could be developed which would account for the inherent uncertainties in a more rational manner.

As a step towards this goal, Arbocz (1984) published the results of an extensive numerical study of the well characterized stringer stiffened shell AS-2, which has been tested at Caltech in 1970 (Singer et al., 1971). Using an early finite difference version of the well-known nonlinear shell code STAGS (Almroth et al., 1971a), the complete shell was modeled. The measured initial imperfections were fitted by a bivariate cubic spline fit. This model was then used to compute the first derivatives of the measured initial imperfection with respect to x and y at all nodal points in a user written subroutine. Employing C-4 ($u = u_0$, $v = w = w_{,x} = 0$) boundary conditions, the nonlinear solution then located the limit point of the prebuckling states. The calculated collapse load of $\rho_s = 0.8563$ is unexpectedly high since the shell AS-2 buckled at $\rho_{exp} = 0.705$, whereby both buckling loads have been normalized by -320.8 N/cm, the buckling load of the perfect shell using membrane prebuckling and the same C-4 boundary conditions.

In looking for an explanation, a comparison of the calculated prebuckling deformation for C-4 boundary condition (see Fig. 2) with the experimentally measured prebuckling deformation (see Fig. 3) is helpful. Obviously, the two deformation patterns are strikingly different. As the measured initial imperfections are modeled quite accurately by the bivariate cubic spline fit used, therefore the answer must be sought in a possible difference between the C-4 boundary conditions used with the numerical calculations and the actual boundary conditions present at the experimental test setup. This statement is reinforced by the results of the flatness survey of one of the end-rings used in the test setup of shell AS-2 shown in Fig. 4. It is obvious that in this case, the condition $u = u_0$ used in the C-4 boundary conditions should be replaced

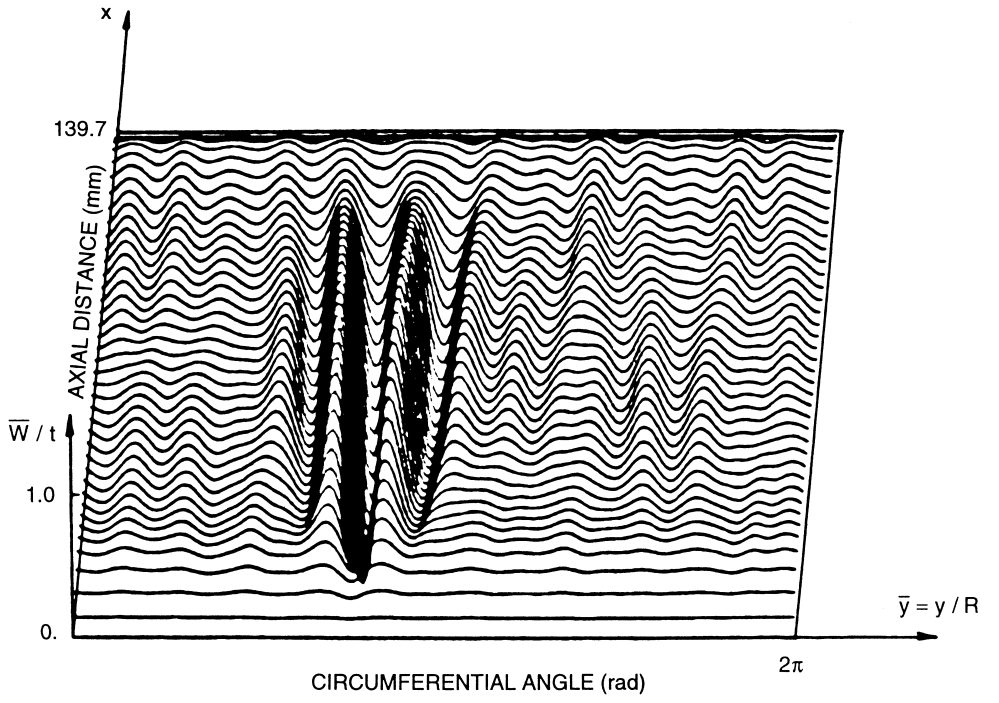

Fig. 2. Calculated prebuckling growth of the stringer stiffened shell AS-2 at $\rho_s = 0.8563$ (Arbocz, 1984) – boundary conditions: $u = u_0$, $v = w = w_{,x} = 0$.

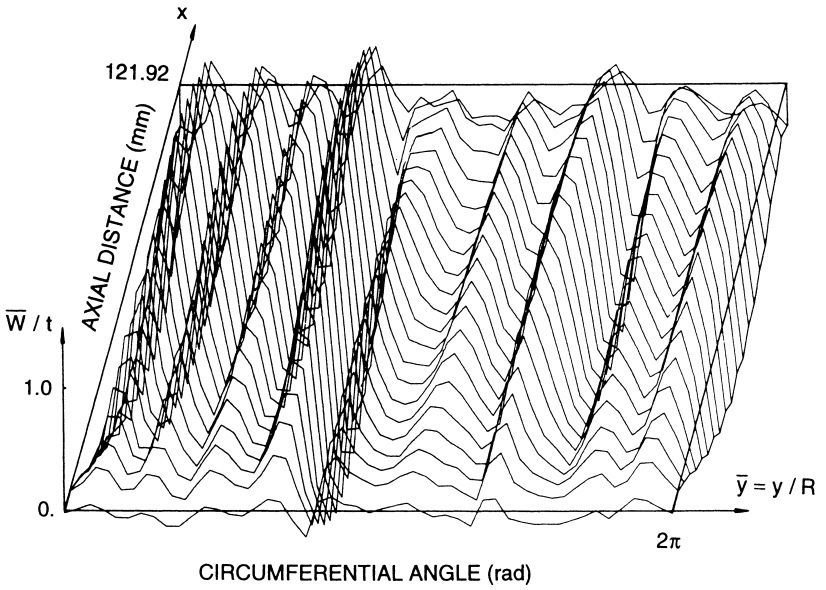

Fig. 3. Measured prebuckling growth of the stringer stiffened shell AS-2 at $\rho = 0.629$ (Singer et al., 1971).

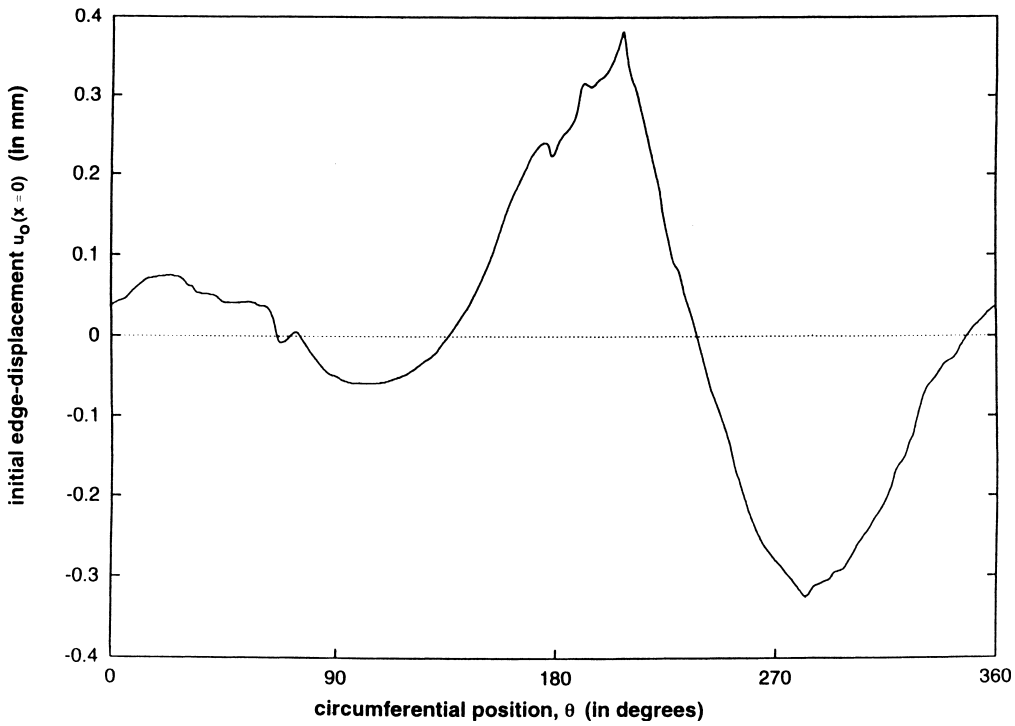

Fig. 4. Measured flatness of the Caltech end-ring (in mm).

by a condition, which allows for a variation of the axial displacement, u in the circumferential direction at the shell edges.

2. Theoretical analysis

In order to gain an insight into the possible interaction between various types of boundary conditions and initial geometric imperfections, at first an analytical investigation is carried out. Using the sign convention defined in Fig. 5, the Donnell-type imperfect anisotropic shell equations (Tennyson and Muggeridge, 1969) can be written as

$$L_{A^*}(F) - L_{B^*}(W) = -(1/R)W_{,xx} - (1/2)L_{\mathrm{NL}}(W, W + 2\overline{W}), \tag{2}$$

$$L_{B^*}(F) + L_{D^*}(W) = (1/R)F_{,xx} + L_{\mathrm{NL}}(F, W + \overline{W}) + p, \tag{3}$$

where the linear operators are

$$\begin{aligned} L_{A^*}(\ ) &= A^*_{22}(\ )_{,xxxx} - 2A^*_{26}(\ )_{,xxxy} + (2A^*_{12} + A^*_{66})(\ )_{,xxyy} - 2A^*_{16}(\ )_{,xyyy} + A^*_{11}(\ )_{,yyyy}, \\ L_{B^*}(\ ) &= B^*_{21}(\ )_{,xxxx} + (2B^*_{26} - B^*_{61})(\ )_{,xxxy} + (B^*_{11} + B^*_{22} - 2B^*_{66})(\ )_{,xxyy} \\ &\quad + (2B^*_{16} - B^*_{62})(\ )_{,xyyy} + B^*_{12}(\ )_{,yyyy}, \\ L_{D^*}(\ ) &= D^*_{11}(\ )_{,xxxx} + 4D^*_{16}(\ )_{,xxxy} + 2(D^*_{12} + 2D^*_{66})(\ )_{,xxyy} + 4D^*_{26}(\ )_{,xyyy} + D^*_{22}(\ )_{,yyyy}, \end{aligned} \tag{4}$$

and the nonlinear operator is

$$L_{\mathrm{NL}}(S, T) = S_{,xx}\,T_{,yy} - 2S_{,xy}\,T_{,xy} + S_{,yy}\,T_{,xx}, \tag{5}$$

where commas in the subscripts denote repeated partial differentiation with respect to the independent variables following the comma. The stiffness parameters $A^*_{11}, B^*_{11}, D^*_{11}, A^*_{12}, \ldots$ are defined in Arbocz and Hol

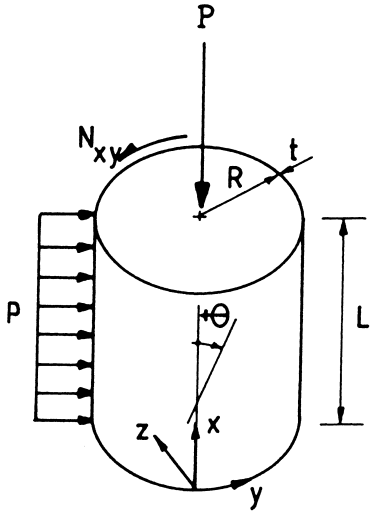

Fig. 5. Notation and sign convention.

(1989). W is the component of the displacement normal to the shell midsurface, $\overline{W}$, the initial radial imperfection (here both positive inward) and F, the Airy stress function.

2.1. Reduction to an equivalent set of ordinary differential equations

If we assume that the initial imperfection is represented as

$$\overline{W}(\overline{x},\overline{y}) = tA_0(\overline{x}) + A_1(\overline{x})\cos n\overline{y} + A_2(\overline{x})\sin n\overline{y}, \tag{6}$$

where $A_0(\overline{x}), A_1(\overline{x}), A_2(\overline{x})$ are known functions of $\overline{x}$, then Eqs. (2) and (3) admit separable solutions of the form

$$W = t(W_v + W_p + W_t) + tw_0(\overline{x}) + tw_1(\overline{x})\cos n\overline{y} + tw_2(\overline{x})\sin n\overline{y}, \tag{7}$$

$$\begin{aligned} F = (ERt^2/c)[&-(1/2)\lambda\overline{y}^2 - (1/2)\overline{p}\,\overline{x}^2 - \overline{\tau}\,\overline{x}\,\overline{y} + f_0(\overline{x}) \\ &+ f_1(\overline{x})\cos n\overline{y} + f_2(\overline{x})\cos 2n\overline{y} + f_3(\overline{x})\sin n\overline{y} + f_4(\overline{x})\sin 2n\overline{y}], \end{aligned} \tag{8}$$

where $\overline{x} = x/R, \overline{y} = y/R$, λ is the nondimensional axial load parameter ($\lambda = (cR/Et^2)N_0$), $\overline{p}$, the nondimensional external pressure ($\overline{p} = (cR^2/Et^2)p$) and $\overline{\tau}$, the nondimensional torque parameter ($\overline{\tau} = (cR/Et^2)N_{xy}$), positive counter-clockwise. The quantities W_v, W_p and W_t are evaluated by enforcing the circumferential periodicity condition (see Appendix A for details).

Substituting the expressions for $\overline{W}$, W and F into the compatibility equation (2), using some trigonometric identities, and finally equating coefficients of like terms, results in the following system of five nonlinear ordinary differential equations:

$$\begin{aligned} &\overline{A}^*_{22}f_0^{\mathrm{iv}} - (1/2)(t/R)\overline{B}^*_{21}w_0^{\mathrm{iv}} + cw_0'' - (c/4)(t/R)n^2 \\ &\quad\times\{w_1''(w_1+2A_1) + 2w_1'(w_1'+2A_1') + w_1(w_1''+2A_1'') \\ &\quad + w_2''(w_2+2A_2) + 2w_2'(w_2'+2A_2') + w_2(w_2''+2A_2'')\} = 0, \end{aligned} \tag{9}$$

$$\begin{aligned} &\overline{A}^*_{22}f_1^{\mathrm{iv}} - n^2(2\overline{A}^*_{12} + \overline{A}^*_{66})f_1'' + n^4\overline{A}^*_{11}f_1 - 2n\overline{A}^*_{26}f_3''' + 2n^3\overline{A}^*_{16}f_3' - (1/2)(t/R) \\ &\quad\times\{\overline{B}^*_{21}w_1^{\mathrm{iv}} - n^2(\overline{B}^*_{11} + \overline{B}^*_{22} - 2\overline{B}^*_{66})w_1'' + n^4\overline{B}^*_{12}w_1 + n(2\overline{B}^*_{26} - \overline{B}^*_{61})w_2''' - n^3(2\overline{B}^*_{16} - \overline{B}^*_{62})w_2'\} \\ &\quad + cw_1'' - (c/2)(t/R)n^2\{w_0''(w_1+2A_1) + w_1(w_0''+2A_0'')\} = 0, \end{aligned} \tag{10}$$

$$\begin{aligned} &\overline{A}^*_{22}f_2^{\mathrm{iv}} - 4n^2(2\overline{A}^*_{12} + \overline{A}^*_{66})f_2'' + 16n^4\overline{A}^*_{11}f_2 - 4n\overline{A}^*_{26}f_4''' + 16n^3\overline{A}^*_{16}f_4' - (c/4)(t/R)n^2 \\ &\quad\times\{w_1''(w_1+2A_1) - 2w_1'(w_1'+2A_1') + w_1(w_1''+2A_1'') - [w_2''(w_2+2A_2) \\ &\quad - 2w_2'(w_2'+2A_2') + w_2(w_2''+2A_2'')]\} = 0, \end{aligned} \tag{11}$$

$$\begin{aligned} &\overline{A}^*_{22}f_3^{\mathrm{iv}} - n^2(2\overline{A}^*_{12} + \overline{A}^*_{66})f_3'' + n^4\overline{A}^*_{11}f_3 + 2n\overline{A}^*_{26}f_1''' - 2n^3\overline{A}^*_{16}f_1'' - (1/2)(t/R) \\ &\quad\times\{\overline{B}^*_{21}w_2^{\mathrm{iv}} - n^2(\overline{B}^*_{11} + \overline{B}^*_{22} - 2\overline{B}^*_{66})w_2'' + n^4\overline{B}^*_{12}w_2 - n(2\overline{B}^*_{26} - \overline{B}^*_{61})w_1''' + n^3(2\overline{B}^*_{16} - \overline{B}^*_{62})w_1'\} \\ &\quad + cw_2'' - (c/2)(t/R)n^2\{w_0''(w_2+2A_2) + w_2(w_0''+2A_0'')\} = 0, \end{aligned} \tag{12}$$

$$\begin{aligned} &\overline{A}^*_{22}f_4^{\mathrm{iv}} - 4n^2(2\overline{A}^*_{12} + \overline{A}^*_{66})f_4'' + 16n^4\overline{A}^*_{11}f_4 + 4n\overline{A}^*_{26}f_2''' - 16n^3\overline{A}^*_{16}f_2' - (c/4)(t/R)n^2 \\ &\quad\times\{w_2''(w_1+2A_1) - 2w_2'(w_1'+2A_1') + w_2(w_1''+2A_1'') + w_1''(w_2+2A_2) \\ &\quad - 2w_1'(w_2'+2A_2') + w_1(w_2''+2A_2'')\} = 0. \end{aligned} \tag{13}$$

The nondimensional stiffness parameters $\overline{A}^*_{11}, \overline{B}^*_{11}, \overline{D}^*_{11}, \ldots$ are listed in Arbocz and Hol (1989). Note that Eq. (9) can be integrated twice yielding

$$\overline{A}^*_{22} f_0'' - (1/2)(t/R)\overline{B}^*_{21} w_0'' + c w_0 - (c/4)(t/R)n^2\{w_1(w_1 + 2A_1) + w_2(w_2 + 2A_2)\} = \tilde{C}_1 \overline{x} + \tilde{C}_2, \tag{14}$$

where $c = \sqrt{3(1-\nu^2)}$, $(\ )' = R(\ )_{,x}$ and the constants of integration $\tilde{C}_1$ and $\tilde{C}_2$ are identically equal to zero because of the periodicity condition (see Appendix A for details).

Substituting in turn the expressions assumed for $\overline{W}$, W and F into the equilibrium equation (3) and applying Galerkin's procedure yields the following system of three nonlinear ordinary differential equations

$$\begin{aligned}
&\overline{B}^*_{21} f_0^{\mathrm{iv}} + (1/2)(t/R)\overline{D}^*_{11} w_0^{\mathrm{iv}} - 2c(R/t) f_0'' + 2c\lambda(w_0'' + A_0'') \\
&\quad + cn^2\{f_1''(w_1 + A_1) + 2f_1'(w_1' + A_1') + f_1(w_1'' + A_1'') \\
&\quad + f_3''(w_2 + A_2) + 2f_3'(w_2' + A_2') + f_3(w_2'' + A_2'')\} = 0,
\end{aligned} \tag{15}$$

$$\begin{aligned}
&\overline{B}^*_{21} f_1^{\mathrm{iv}} - n^2(\overline{B}^*_{11} + \overline{B}^*_{22} - 2\overline{B}^*_{66}) f_1'' + n^4 \overline{B}^*_{12} f_1 + n(2\overline{B}^*_{26} - \overline{B}^*_{61}) f_3''' - n^3(2\overline{B}^*_{16} - \overline{B}^*_{62}) f_3' \\
&\quad + (1/2)(t/R)\{\overline{D}^*_{11} w_1^{\mathrm{iv}} - 2n^2(\overline{D}^*_{12} + 2\overline{D}^*_{66}) w_1'' + n^4 \overline{D}^*_{22} w_1 + 4n\overline{D}^*_{16} w_2''' - 4n^3 \overline{D}^*_{26} w_2'\} \\
&\quad - 2c(R/t) f_1'' + 2c\lambda(w_1'' + A_1'') - 2cn^2 \overline{p}(w_1 + A_1) - 4cn\overline{\tau}(w_2' + A_2') + 2cn^2\{f_0''(w_1 + A_1) + f_1(w_0'' + A_0'')\} \\
&\quad + cn^2\{f_2''(w_1 + A_1) + 4f_2'(w_1' + A_1') + 4f_2(w_1'' + A_1'') + f_4''(w_2 + A_2) + 4f_4'(w_2' + A_2') \\
&\quad + 4f_4(w_2'' + A_2'')\} = 0,
\end{aligned} \tag{16}$$

$$\begin{aligned}
&\overline{B}^*_{21} f_3^{\mathrm{iv}} - n^2(\overline{B}^*_{11} + \overline{B}^*_{22} - 2\overline{B}^*_{66}) f_3'' + n^4 \overline{B}^*_{12} f_3 - n(2\overline{B}^*_{26} - \overline{B}^*_{61}) f_1''' + n^3(2\overline{B}^*_{16} - \overline{B}^*_{62}) f_1' \\
&\quad + (1/2)(t/R)\{\overline{D}^*_{11} w_2^{\mathrm{iv}} - 2n^2(\overline{D}^*_{12} + 2\overline{D}^*_{66}) w_2'' + n^4 \overline{D}^*_{22} w_2 - 4n\overline{D}^*_{16} w_1''' + 4n^3 \overline{D}^*_{26} w_1'\} \\
&\quad - 2c(R/t) f_3'' + 2c\lambda(w_2'' + A_2'') - 2cn^2 \overline{p}(w_2 + A_2) + 4cn\overline{\tau}(w_1' + A_1') + 2cn^2\{f_0''(w_2 + A_2) + f_3(w_0'' + A_0'')\} \\
&\quad + cn^2\{f_4''(w_1 + A_1) + 4f_4'(w_1' + A_1') + 4f_4(w_1'' + A_1'') - [f_2''(w_2 + A_2) + 4f_2'(w_2' + A_2') \\
&\quad + 4f_2(w_2'' + A_2'')]\} = 0.
\end{aligned} \tag{17}$$

With the help of Eqs. (9) and (14), one can eliminate the terms f_0^{iv} and f_0'' from the other equations. Further, in order to be able to use the "parallel shooting method" of Keller (1968) for numerical solution of the above system of nonlinear ordinary differential equations, it is necessary to reformulate Eqs. (10)–(17) so that only a single fourth derivative appears on the left-hand side. This can be accomplished by using Eqs. (16), (17), (10) and (12) to eliminate the terms w_1^{iv}, w_2^{iv}, f_1^{iv} and f_3^{iv} from Eqs. (10), (12), (16) and (17), respectively. Finally, some further regrouping makes it possible to write the resulting equations as

$$\begin{aligned}
f_1^{\mathrm{iv}} &= C_1 f_1'' - C_2 f_1 - C_3 w_1'' - C_4\lambda(w_1'' + A_1'') + C_5 w_1 \\
&\quad + C_{201} f_3''' - C_{202} f_3' + C_{203} w_2''' - C_{204} w_2' + C_{211}\overline{p}(w_1 + A_1) \\
&\quad + C_{212}\overline{\tau}(w_2' + A_2') + C_6[w_0''(w_1 + 2A_1) + w_1(w_0'' + 2A_0'')] - C_7 w_0''(w_1 + A_1) \\
&\quad + C_8 w_0(w_1 + A_1) - C_9[w_1(w_1 + 2A_1) + w_2(w_2 + 2A_2)](w_1 + A_1) - 2C_{10} f_1(w_0'' + A_0'') \\
&\quad - C_{10}\{f_2''(w_1 + A_1) + 4f_2'(w_2' + A_2') + 4f_2(w_1'' + A_1'') + f_4''(w_2 + A_2) + 4f_4'(w_2' + A_2') + 4f_4(w_2'' + A_2'')\},
\end{aligned} \tag{18}$$

$$\begin{aligned}
f_2^{\mathrm{iv}} &= C_{11} f_2'' - C_{12} f_2 + C_{205} f_4'''' - C_{206} f_4' \\
&\quad + C_{13}\{w_1''(w_1 + 2A_1) - 2w_1'(w_1' + 2A_1') + w_1(w_1'' + 2A_1'') \\
&\quad - [w_2''(w_2 + 2A_2) - 2w_2'(w_2' + 2A_2') + w_2(w_2'' + 2A_2'')]\},
\end{aligned} \tag{19}$$

$$
\begin{aligned}
f_3^{\mathrm{iv}} &= C_1 f_3'' - C_2 f_3 - C_3 w_2'' - C_4\lambda(w_2'' + A_2'') + C_5 w_2 \\
&\quad - C_{201} f_1''' + C_{202} f_1' - C_{203} w_1''' + C_{204} w_1' + C_{211}\overline{p}(w_2 + A_2) \\
&\quad - C_{212}\overline{\tau}(w_1' + A_1') + C_6[w_0''(w_2 + 2A_2) + w_2(w_0'' + 2A_0'')] - C_7 w_0''(w_2 + A_2) \\
&\quad + C_8 w_0(w_2 + A_2) - C_9[w_1(w_1 + 2A_1) + w_2(w_2 + 2A_2)](w_2 + A_2) - 2C_{10} f_3(w_0'' + A_0'') \\
&\quad - C_{10}\{f_4''(w_1 + A_1) + 4f_4'(w_1' + A_1') + 4f_4(w_1'' + A_1'') - [f_2''(w_2 + A_2) + 4f_2'(w_2' + A_2') \\
&\qquad + 4f_2(w_2'' + A_2'')]\},
\end{aligned} \tag{20}
$$

$$
\begin{aligned}
f_4^{\mathrm{iv}} &= C_{11} f_4'' - C_{12} f_4 - C_{205} f_2''' + C_{206} f_2' \\
&\quad + C_{13}\{w_2''(w_1 + 2A_1) - 2w_2'(w_1' + 2A_1') + w_2(w_1'' + 2A_1'') \\
&\qquad + w_1''(w_2 + 2A_2) - 2w_1'(w_2' + 2A_2') + w_1(w_2'' + 2A_2'')\},
\end{aligned} \tag{21}
$$

$$
\begin{aligned}
w_0^{\mathrm{iv}} &= C_{14} w_0'' - C_{15} w_0 - C_{19}\lambda(w_0'' + A_0'') + C_{17}[w_1(w_1 + 2A_1) + w_2(w_2 + 2A_2)] \\
&\quad - C_{16}\{w_1''(w_1 + 2A_1) + 2w_1'(w_1' + 2A_1') + w_1(w_1'' + 2A_1'') \\
&\qquad + w_2''(w_2 + 2A_2) + 2w_2'(w_2' + 2A_2') + w_2(w_2'' + 2A_2'')\} \\
&\quad - C_{18}\{f_1''(w_1 + A_1) + 2f_1'(w_1' + A_1') + f_1(w_1'' + A_1'') + f_3''(w_2 + A_2) + 2f_3'(w_2' + A_2') + f_3(w_2'' + A_2'')\},
\end{aligned} \tag{22}
$$

$$
\begin{aligned}
w_1^{\mathrm{iv}} &= C_{20} w_1'' - C_{21} w_1 + C_{22} f_1'' - C_{24} f_1 - C_{23}\lambda(w_1'' + A_1'') \\
&\quad - C_{209} w_2''' + C_{210} w_2' - C_{207} f_3''' + C_{208} f_3' + C_{213}\overline{p}(w_1 + A_1) \\
&\quad + C_{214}\overline{\tau}(w_2' + A_2') - C_{25}[w_0''(w_1 + 2A_1) + w_1(w_0'' + 2A_0'')] - C_{26} w_0''(w_1 + A_1) \\
&\quad + C_{27} w_0(w_1 + A_1) - C_{28}[w_1(w_1 + 2A_1) + w_2(w_2 + 2A_2)](w_1 + A_1) - 2C_{29} f_1(w_0'' + A_0'') \\
&\quad - C_{29}\{f_2''(w_1 + A_1) + 4f_2'(w_1' + A_1') + 4f_2(w_1'' + A_1'') + f_4''(w_2 + A_2) + 4f_4'(w_2' + A_2') + 4f_4(w_2'' + A_2'')\},
\end{aligned} \tag{23}
$$

$$
\begin{aligned}
w_2^{\mathrm{iv}} &= C_{20} w_2'' - C_{21} w_2 + C_{22} f_3'' - C_{24} f_3 - C_{23}\lambda(w_2'' + A_2'') \\
&\quad + C_{209} w_1''' - C_{210} w_1' + C_{207} f_1''' - C_{208} f_1' + C_{213}\overline{p}(w_2 + A_2) \\
&\quad - C_{214}\overline{\tau}(w_1' + A_1') - C_{25}[w_0''(w_2 + 2A_2) + w_2(w_0'' + 2A_0'')] - C_{26} w_0''(w_2 + A_2) \\
&\quad + C_{27} w_0(w_2 + A_2) - C_{28}[w_1(w_1 + 2A_1) + w_2(w_2 + 2A_2)](w_2 + A_2) - 2C_{29} f_3(w_0'' + A_0'') \\
&\quad - C_{29}\{f_4''(w_1 + A_1) + 4f_4'(w_1' + A_1') + 4f_4(w_1'' + A_1'') - f_2''(w_2 + A_2) + 4f_2'(w_2' + A_2') \\
&\qquad + 4f_2(w_2'' + A_2'')\}.
\end{aligned} \tag{24}
$$

The constants C_1–C_{214} are listed in Arbocz et al. (1998). Note that by assuming the axial dependence of the response to be an unknown function of $\overline{x}$, the buckling problem is reduced to the solution of a set of nonlinear ordinary differential equations, which will allow the rigorous enforcing of the specified boundary conditions.

2.2. Derivation of the reduced boundary conditions

To complete the mathematical formulation of the stability problem, one has to express the specified boundary conditions in terms of the dependent variables F and W. The derivation of these so-called reduced boundary conditions will be illustrated with one of the admissible in-plane boundary conditions, namely

$$u = u_b(y) = t\overline{u}_0 + t\overline{u}_1 \cos n\overline{y} + t\overline{u}_2 \cos 2n\overline{y} + t\overline{u}_3 \sin n\overline{y} + t\overline{u}_4 \sin 2n\overline{y}. \tag{25}$$

Eliminating v between the following Donnell type strain–displacement relations

$$\varepsilon_y = v_{,y} - (1/R)W + (1/2)W_{,y}^2 + \overline{W}_{,y} W_{,y}\,, \tag{26}$$

$$\gamma_{xy} = u_{,y} + v_{,x} + W_{,x} W_{,y} + \overline{W}_{,x} W_{,y} + W_{,x} \overline{W}_{,y}\,, \tag{27}$$

one obtains

$$\gamma_{xy,y} - \varepsilon_{y,x} = u_{,yy} + (1/R)W_{,x} + W_{,x} W_{,yy} + \overline{W}_{,x} W_{,yy} + W_{,x} \overline{W}_{,yy}\,. \tag{28}$$

Introducing the semi-inverted constitutive equations for γ_{xy} and ε_y and specializing the resulting expressions to the shell edges (at $\overline{x} = 0$ and $\overline{x} = L/R$) yields

$$\begin{aligned}
&(1/Et)\{-\overline{A}_{22}^* F_{,xxx} + 2\overline{A}_{26}^* F_{,xxy} - (\overline{A}_{12}^* + \overline{A}_{66}^*) F_{,xyy} + \overline{A}_{16}^* F_{,yyy}\} + (t/2c) \\
&\quad \times \{\overline{B}_{21}^* W_{,xxx} + (2\overline{B}_{26}^* - \overline{B}_{61}^*) W_{,xxy} + (\overline{B}_{22}^* - 2\overline{B}_{66}^*) W_{,xyy} - \overline{B}_{62}^* W_{,yyy}\} \\
&\quad = -(n^2/R^2)t\{\overline{u}_1 \cos n\overline{y} + 4\overline{u}_2 \cos 2n\overline{y} + \overline{u}_3 \sin n\overline{y} + \overline{u}_4 \sin 2n\overline{y}\} \\
&\qquad + (1/R)W_{,x} + W_{,x} W_{,yy} + \overline{W}_{,x} W_{,yy} + W_{,x} \overline{W}_{,yy}\,.
\end{aligned} \tag{29}$$

Substituting for $\overline{W}$, W and F from Eqs. (6)–(8), regrouping and equating coefficients of like terms yields the following expressions:

$$\begin{aligned}
&\overline{A}_{22}^* f_0''' - (1/2)(t/R)\overline{B}_{21}^* w_0''' + c w_0' \\
&\quad - (c/2)(t/R)n^2\{w_1'(w_1 + A_1) + w_1 A_1' + w_2'(w_2 + A_2) + w_2 A_2'\} = 0,
\end{aligned} \tag{30}$$

$$\begin{aligned}
&\overline{A}_{22}^* f_1''' - (\overline{A}_{12}^* + \overline{A}_{66}^*)n^2 f_1' - 2\overline{A}_{26}^* n f_3'' + \overline{A}_{16}^* n^3 f_3 + c w_1' - c(t/R)n^2[w_0'(w_1 + A_1) + w_1 A_0'] \\
&\quad - (1/2)(t/R)\{\overline{B}_{21}^* w_1''' - (\overline{B}_{22}^* - 2\overline{B}_{66}^*)n^2 w_1' + (2\overline{B}_{26}^* - \overline{B}_{61}^*)n w_2'' + \overline{B}_{62}^* n^3 w_2\} - c n^2 \overline{u}_1 = 0,
\end{aligned} \tag{31}$$

$$\begin{aligned}
&\overline{A}_{22}^* f_2''' - (\overline{A}_{12}^* + \overline{A}_{66}^*)4n^2 f_2' - 4\overline{A}_{26}^* n f_4'' + 8\overline{A}_{16}^* n^3 f_4 \\
&\quad - (c/2)(t/R)n^2\{w_1'(w_1 + A_1) + w_1 A_1' - [w_2'(w_2 + A_2) + w_2 A_2']\} - 4c n^2 \overline{u}_2 = 0,
\end{aligned} \tag{32}$$

$$\begin{aligned}
&\overline{A}_{22}^* f_3''' - (\overline{A}_{12}^* + \overline{A}_{66}^*)n^2 f_3' + 2\overline{A}_{26}^* n f_1'' - \overline{A}_{16}^* n^3 f_1 + c w_2' - c(t/R)n^2[w_0'(w_2 + A_2) + w_2 A_0'] \\
&\quad - (1/2)(t/R)\{\overline{B}_{21}^* w_2''' - (\overline{B}_{22}^* - 2\overline{B}_{66}^*)n^2 w_2' - (2\overline{B}_{26}^* - \overline{B}_{61}^*)n w_1'' - \overline{B}_{62}^* n^3 w_1] - c n^2 \overline{u}_3 = 0,
\end{aligned} \tag{33}$$

$$\begin{aligned}
&\overline{A}_{22}^* f_4''' - (\overline{A}_{12}^* + \overline{A}_{66}^*)4n^2 f_4' + 4\overline{A}_{26}^* n f_2'' - 8\overline{A}_{16}^* n^3 f_2 \\
&\quad - (c/2)(t/R)n^2\{w_1'(w_2 + A_2) + w_1 A_2' + w_2'(w_1 + A_1) + w_2 A_1'\} - 4c n^2 \overline{u}_4 = 0.
\end{aligned} \tag{34}$$

Notice that the first of these expressions, Eq. (30) does not represent a new (boundary) condition as it can be obtained from Eq. (14) by a single differentiation with respect to $\overline{x}$. A complete list of the reduced boundary conditions and further details of the derivation can be found in Arbocz et al. (1998).

3. Numerical analysis

Due to the highly nonlinear nature of the stability problem represented by Eqs. (18)–(24) and the appropriate boundary conditions a numerical solution is called for. All the known numerical techniques for the solution of nonlinear equations involve iterative improvements of initial guesses of the solution. Working with isotropic (Arbocz and Sechler, 1974) and orthotropic (Arbocz and Sechler, 1976) shells, it

was found that the method known as "parallel shooting" (Keller, 1968) works very well for this type of problems. This method can be best formulated in terms of a first-order vector differential equation.

3.1. Formulation of the 2-point boundary value problem

Introducing, as a unified variable, the 28-dimensional vector $\underset{\sim}{Y}$ defined as follows:

$$\begin{aligned}
&Y_1 = f_1, \quad Y_2 = f_2, \quad Y_3 = f_3, \quad Y_4 = f_4, \quad Y_5 = w_0, \quad Y_6 = w_1, \quad Y_7 = w_2,\\
&Y_8 = f_1', \quad Y_9 = f_2', \quad Y_{10} = f_3', \quad Y_{11} = f_4', \quad Y_{12} = w_0', \quad Y_{13} = w_1', \quad Y_{14} = w_2',\\
&Y_{15} = f_1'', \quad Y_{16} = f_2'', \quad Y_{17} = f_3'', \quad Y_{18} = f_4'', \quad Y_{19} = w_0'', \quad Y_{20} = w_1'', \quad Y_{21} = w_2'',\\
&Y_{22} = f_1''', \quad Y_{23} = f_2''', \quad Y_{24} = f_3''', \quad Y_{25} = f_4''', \quad Y_{26} = w_0''', \quad Y_{27} = w_1''', \quad Y_{28} = w_2''',
\end{aligned} \tag{35}$$

and using the SS-4 boundary conditions ($u = u_b, v = W = M_x = 0$) as an illustration, which in terms of the assumed unknown functions become

$$\begin{aligned}
u = u_b \rightarrow f_1''' &= B_{28} f_1' - B_{29} f_3 + B_8 w_1''' + B_{30} w_1' + 2B_9 A_1 w_0' + c(n^2/\overline{A}_{22}^*)\overline{u}_1,\\
f_2''' &= 4B_{31} f_2' - 8B_{32} f_4 + B_9 A_1 w_1' - B_9 A_2 w_2' + 4c(n^2/\overline{A}_{22}^*)\overline{u}_2,\\
f_3''' &= B_{28} f_3' + B_{29} f_1 + B_8 w_2''' + B_{30} w_2' + 2B_9 A_2 w_0' + c(n^2/\overline{A}_{22}^*)\overline{u}_3,\\
f_4''' &= 4B_{31} f_4' + 8B_{32} f_2 + B_9 A_2 w_1' + B_9 A_1 w_2' + 4c(n^2/\overline{A}_{22}^*)\overline{u}_4,
\end{aligned} \tag{36}$$

$$\begin{aligned}
v = 0 \rightarrow f_1'' &= B_{20} f_1 + B_{15} f_3' + B_{16} w_2',\\
f_2'' &= 4B_{24} f_2 + 2B_{17} f_4',\\
f_3'' &= B_{20} f_3 - B_{15} f_1' - B_{16} w_1',\\
f_4'' &= 4B_{24} f_4 - 2B_{17} f_2',
\end{aligned} \tag{37}$$

$$\begin{aligned}
W = 0 \rightarrow w_0 &= -(W_v + W_p + W_t),\\
w_1 &= w_2 = 0,
\end{aligned} \tag{38}$$

$$\begin{aligned}
M_x = 0 \rightarrow w_0'' &= C_{41}\lambda + C_{220}\overline{\tau},\\
w_1'' &= B_{25} f_1 + B_{18} f_3' - B_{19} w_2',\\
w_2'' &= B_{25} f_3 - B_{18} f_1' + B_{19} w_1',
\end{aligned} \tag{39}$$

then the system of Eqs. (18)–(24) can be reduced to the following nonlinear 2-point boundary value problem

$$\frac{\mathrm{d}}{\mathrm{d}\overline{x}}\underset{\sim}{Y} = \underset{\sim}{f}(\overline{x}, \underset{\sim}{Y}; \lambda, \overline{p}, \overline{\tau}) \quad \text{for } 0 \leqslant \overline{x} \leqslant L/R, \tag{40}$$

$$\begin{aligned}
\overline{\overline{B}}_0 \underset{\sim}{Y}(\overline{x} = 0) &= \underset{\sim}{\alpha} \quad \text{at } \overline{x} = 0,\\
\overline{\overline{B}}_1 \underset{\sim}{Y}(\overline{x} = L/R) &= \underset{\sim}{\beta} \quad \text{at } \overline{x} = L/R,
\end{aligned} \tag{41}$$

where the components of the 14×28 matrices $\overline{\overline{B}}_0$ and $\overline{\overline{B}}_1$ depend on the specified boundary conditions at the shell edges. The constants $B_1, B_2, \ldots B_{32}$ used in the definition of the boundary conditions are listed in Arbocz et al. (1998).

The solution of this nonlinear 2-point boundary value problem will locate the limit point of the prebuckling states. The applied loading consists of an axial compression, internal or external pressure and clockwise or counter-clockwise torque. It is assumed to have a uniform spatial distribution and is divided into a fixed part and a variable part. The magnitude of the variable part is allowed to vary in proportion to a load parameter Λ. By definition, the value of the loading parameter Λ corresponding to the limit point will be the theoretical buckling load (see also Fig. 6). In Eq. (40), the user can select Λ to be the critical value of either the normalized axial load λ, or the normalized external pressure $\overline{p}$ or the normalized torque $\overline{\tau}$.

Considering the results presented in Fig. 6, where the maximum amplitude of the asymmetric component of the prebuckling deformation is plotted versus the normalized axial load level, one observes that using load increments, the solution fails to converge close to and beyond the limit point. This situation is unsatisfactory, especially, since without the appropriate starting values the nonlinear iteration scheme will fail to converge also at load levels less than the theoretical buckling load. A closer look at the solution curve presented in Fig. 6 reveals, however, that one should be able to extend the response curve beyond the limit point by using increments in deformation instead of increments in loading. In this case, the load parameter Λ becomes an additional unknown; thus, one needs an extra equation.

Following Kempner (1954), let us define "unit end-shortening" as

$$\varepsilon = \frac{1}{2\pi RL}\int_0^{2\pi R}(u_{,x} - qW_{,xx})\,\mathrm{d}x\,\mathrm{d}y, \tag{42}$$

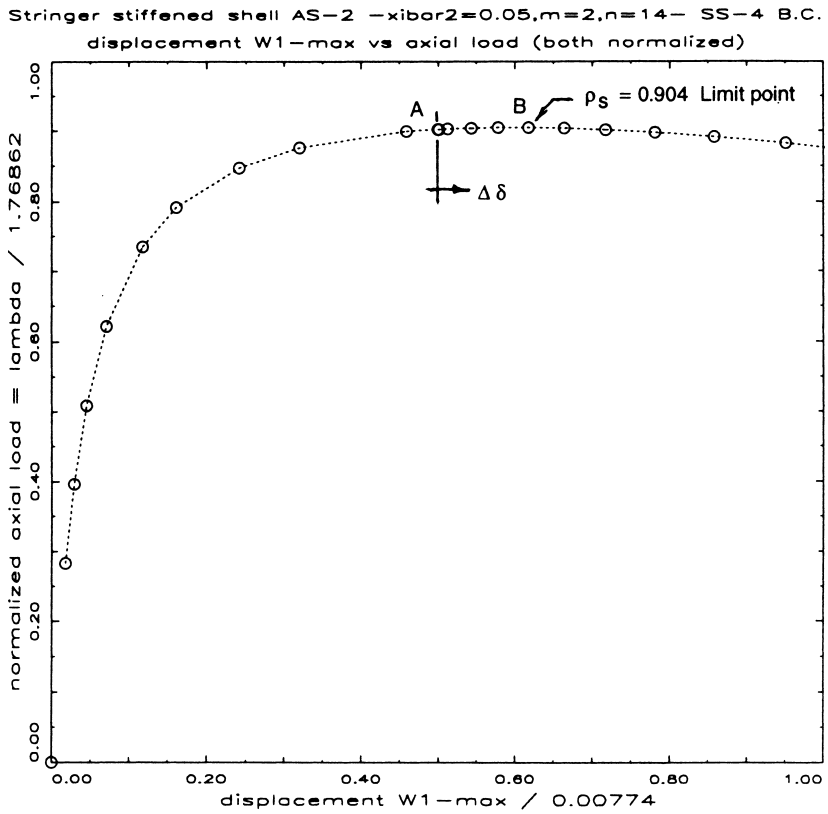

Fig. 6. Variation of $|w_{1\,\max}|$ with axial load.

where

$$u_{,x} = \varepsilon_x - (1/2)W_{,x}\,(W_{,x} + 2\overline{W}_{,x}\,), \tag{43}$$

$$\varepsilon_x = A^*_{11}F_{,yy} + A^*_{12}F_{,xx} - A^*_{16}F_{,xy} - B^*_{11}W_{,xx} - B^*_{12}W_{,yy} - 2B^*_{16}W_{,xy}\,, \tag{44}$$

and q is the load eccentricity measured from the skin midsurface, positive inward. Introducing Eqs. (43) and (44) into the definition of end-shortening, substituting for $\overline{W}$, W and F from Eqs. (6)–(8), carrying out the y-integration, substituting for f_0'' from Eq. (14), introducing $\varepsilon_{c\ell} = t/(cR)$ and the usual nondimensional parameters yields after some regrouping

$$\begin{aligned}\delta = \varepsilon/\varepsilon_{c\ell} = {} & \overline{A}^*_{11}\lambda + \overline{A}^*_{12}\overline{p} - \overline{A}^*_{16}\overline{\tau} \\ & + \int_0^{L/R} \langle C_{50}w_0'' + C_{51}w_0 - C_{52}[w_1(w_1 + 2A_1) + w_2(w_2 + 2A_2)] \\ & + C_{53}\{w_0'(w_0' + 2A_0') + (1/2)[w_1'(w_1' + 2A_1') + w_2'(w_2' + 2A_2')]\}\rangle \mathrm{d}\overline{x},\end{aligned} \tag{45}$$

where the terms involving the integral represent the nonlinear part of the end-shortening δ_{nl}. When solving the boundary value problem of Eq. (40), it is advantageous to solve for δ_{nl} by solving the associated initial value problem, rather than using numerical integration schemes. Here one must solve

$$\begin{aligned}\frac{\mathrm{d}}{\mathrm{d}\overline{x}}\delta_{nl} = {} & C_{50}w_0'' + C_{51}w_0 - C_{52}[w_1(w_1 + 2A_1) + w_2(w_2 + 2A_2)] \\ & + C_{53}\{w_0'(w_0' + 2A_0') + (1/2)[w_1'(w_1' + 2A_1') + w_2'(w_2' + 2A_2')]\},\end{aligned} \tag{46}$$

$$\begin{aligned}\delta_{nl}(\overline{x} = 0) &= 0, \\ \delta_{nl}(\overline{x} = L/R) &= \delta_0,\end{aligned} \tag{47}$$

where δ_0 is the specified nonlinear end-shortening and the constants $C_{50}, C_{51}, \ldots$ are listed in Arbocz et al. (1998). This initial value problem, expressed in terms of the unified vector variable $\underset{\sim}{Y}$, represents the one additional equation needed when solving the 2-point boundary value problem (Eq. (40)) using increments in "end shortening" instead of increments in loading. A detailed description of the "parallel shooting method" used to solve the 2-point boundary value problem is given in Arbocz and Sechler (1974) when using increments in axial load $\Delta\lambda$ and in Arbocz (1975) when using increments in end-shortening $\Delta\delta_{nl}$.

The numerical solution is started at a sufficiently low axial load level λ, so that values from the linearized solution can be used as starting values for the nonlinear iteration scheme. Solutions of the linearized problem are also obtained by the "parallel shooting method" (Arbocz and Sechler, 1973). It is well known that for the linearized 2-point boundary value problem, Newton's method yields the correct initial value $\underset{\sim}{S}$ directly without the need of iterations (Keller, 1968).

The numerical solution of the associated initial value problems and the corresponding variational equations is done by the library subroutine DEQ from Caltech's Willis Booth Computer Center. DEQ uses the method of Runge–Kutta–Gill to compute starting values for an Adams–Moulton corrector–predictor scheme. The program includes an option with variable interval size and uses automatic truncation error control. For the AS-2 shell with an $L/R = 1.375$, parallel shooting over eight intervals is used. For a general anisotropic shell, working with eight intervals actually involves the numerical integration of six 812 dimensional vector equations and two 420 dimensional vector equations. These high dimensions are due to the simultaneous integration of the variational equations and the corresponding associated initial value problems. For proper convergence (say, five digit accuracy) at low load levels, two iterations are sufficient; however, at load levels close to the limit point 6–12 iterations may be needed to obtain the same level of convergence. Thus, upon reaching the load level corresponding to point A in Fig. 6, instead of further increments in the axial load $\Delta\lambda$ increments in the nonlinear end-shortening $\Delta\delta_{nl}$ are used to continue the

solution. This switch in increments makes it possible to integrate around the limit point at B and get converged solutions on the decreasing portion of the solution curve.

4. Numerical results

It has been shown by Singer (1983) that different experimental boundary conditions can have a pronounced effect on the buckling load of stringer stiffened shells. To investigate these effects numerically, initially the buckling loads of the stringer stiffened shell AS-2 (see Fig. 7 for details) for the eight standard sets of boundary conditions introduced by Hoff (1961) are calculated. The shell dimensions and stiffener parameters are summarized in Table 1. Notice that A_1 is the cross-sectional area of the stringer, I_{11}, the moment of inertia of the stringer cross-section about its centroidal axis and I_{t1}, the torsion constant of the stringer cross-section. The definition of the standard boundary conditions for axial compression is given in Table 2. In order to be able to properly assess the effect of imperfect boundary imperfections, it is first necessary to calculate the buckling loads of the corresponding perfect shells.

4.1. Buckling loads of the perfect shell

In order to verify the accuracy of the numerical solutions described earlier in this article, the buckling loads of the perfect stringer stiffened shell AS-2 are calculated for the eight standard sets of boundary conditions given in Table 2. In addition to the buckling loads calculated by the present code called COLLAPSE, Table 3 also contains results obtained by three other codes as indicated.

These other codes initially calculate the axisymmetric nonlinear prebuckling path of the perfect shell and then compute the load level at which bifurcation into an asymmetric pattern will occur. It is the user's responsibility to select the range of circumferential wave numbers n for which the search of the lowest bifurcation buckling load is to be carried out. As a plot of bifurcation buckling load versus circumferential wave numbers may contain several local minima, it requires some engineering insight to ensure that one has located the lowest buckling load.

COLLAPSE, on the contrary, calculates the nonlinear response of an imperfect shell for increasing load levels and determines the limit point of the load carrying capacity. By choosing a vanishingly small asymmetric imperfection amplitude (say, 0.1×10^{-5}), the location of the limit point approaches asymptotically the bifurcation buckling load of the perfect shell.

The ANILISA of Arbocz and Hol (1990) and the present code COLLAPSE both use Donnell-type equations, thus it is not surprising that the agreement between the results obtained is excellent, whereby, as expected, the COLLAPSE results are always slightly lower. The SRA of Cohen (1971) uses Novozhilov

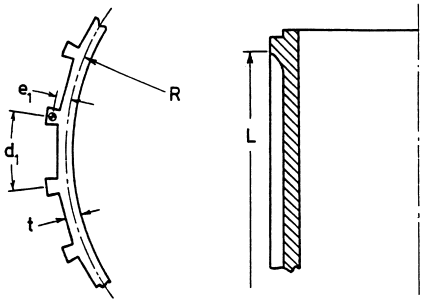

Fig. 7. Geometry of the stringer stiffened shell AS-2 (Singer et al., 1971).

Table 1
Geometric and material properties of the stringer stiffened shell AS-2 (Singer et al., 1971)

$t = 1.96596 \times 10^2$, cm ($=0.00774$, in.)
$L = 13.970$, cm ($=5.50$, in.)
$R = 10.16$, cm ($=4.00$, in.)
$d_1 = 8.03402 \times 10^{-1}$, cm ($=0.3163$, in.)
$e_1 = -3.36804 \times 10^{-2}$, cm ($=-0.01326$, in.)
$A_1 = 7.98708 \times 10^{-3}$, cm^2 ($= 0.1238 \times 10^{-2}$, in.^{2})
$I_{11} = 1.50384 \times 10^{-6}$, cm^4 ($= 0.3613 \times 10^{-7}$, in.^{4})
$I_{t1} = 4.94483 \times 10^{-6}$, cm^4 ($= 0.1188 \times 10^{-6}$, in.^{4})
$E = 6.89472 \times 10^6$, N/cm^2 ($= 10 \times 10^6$, psi)
$v = 0.3$

Table 2
Definition of the standard boundary conditions for axial compression

SS-1	$N_x = -N_0$	$N_{xy} = 0$	$W = 0$	$M_x = -qN_0$
SS-2	$u = u_b$	$N_{xy} = 0$	$W = 0$	$M_x = -qN_0$
SS-3	$N_x = -N_0$	$v = 0$	$W = 0$	$M_x = -qN_0$
SS-4	$u = u_b$	$v = 0$	$W = 0$	$M_x = -qN_0$
C-1	$N_x = -N_0$	$N_{xy} = 0$	$W = 0$	$W_{,x} = 0$
C-2	$u = u_b$	$N_{xy} = 0$	$W = 0$	$W_{,x} = 0$
C-3	$N_x = -N_0$	$v = 0$	$W = 0$	$W_{,x} = 0$
C-4	$u = u_b$	$v = 0$	$W = 0$	$W_{,x} = 0$

Table 3
Normalized perfect shell buckling loads λ_c^{nl} of the stringer stiffened shell AS-2 $A_1/d_1t = 0.506, EI_{11}/d_1D = 2.690, e_1/t = -1.713$ (outside), $GI_{t1}/d_1D = 3.402$[a]

Boundary condition	Arbocz and Hol (1990)	Cohen (1971)	COLLAPSE	Almroth et al. (1973)
SS-1	1.39755 ($n = 10$)	1.37924 ($n = 10$)	1.39748 ($n = 10$)	1.36731 ($n = 10$)
SS-2	1.65546* ($n = 13$)	1.64994* ($n = 13$)	1.65535*($n = 13$)	1.63501*($n = 13$)
SS-3	1.42990 ($n = 10$)	1.41083 ($n = 10$)	1.42983 ($n = 10$)	1.39743 ($n = 10$)
SS-4	1.76862* ($n = 14$)	1.76406* ($n = 14$)	1.76849*($n = 14$)	1.74440*($n = 14$)
C-1	1.61389 ($n = 10$)	1.59340 ($n = 10$)	1.61380 ($n = 10$)	1.57712 ($n = 10$)
C-2	1.99989* ($n = 14$)	1.99616* ($n = 14$)	1.99973*($n = 14$)	1.96676*($n = 14$)
C-3	1.63503 ($n = 10$)	1.61485 ($n = 10$)	1.63494 ($n = 10$)	1.59864 ($n = 10$)
C-4	1.99996* ($n = 14$)	1.99626* ($n = 14$)	1.99981*($n = 14$)	1.96683*($n = 14$)

[a] $\lambda_c^{nl} = N_x/N_{c\ell}$, $N_{c\ell} = -Et^2/cR = -90.6443$ lb/in.; $D = Et^3/4c^2, c = \sqrt{3(1-v^2)}$, $E = 10 \times 10^6$psi, $v = 0.3$; $*=$ buckling mode is antisymmetric with respect to $x = L/2$.

type shell equations and it employs a numerical integration scheme similar to the one used by ANILISA and COLLAPSE. Thus convergence is controlled by the "error bound" specified and the program selects the proper step sizes internally to satisfy it. This eliminates the need for repeated runs with different step sizes to verify convergence, as is the recommended practice with standard finite difference or finite element codes. Finally, STAGS-A of Almroth et al. (1971a) uses a 2-dimensional finite difference based energy formulation with Marlowe–Flügge (Almroth et al., 1971b) type kinematic relations. The results presented are based on a full length shell model where only half of the circumference (thus $\Delta\theta = 180^\circ$) is modeled. Using a mesh consisting of 41 rows and 121 columns results in a nonlinear bifurcation problem with 15 867 degrees of freedom.

Fig. 8 shows the critical buckling mode of the axially compressed stringer stiffened shell AS-2 calculated with COLLAPSE using SS-4 boundary conditions. Notice that the axisymmetric part $t[W_v + w_0(\bar{x})]$ is plotted first, followed by the asymmetric part $t[w_1(\bar{x})\cos n\bar{y} + w_2(\bar{x})\sin n\bar{y}]$, where for an orthotropic shell like AS-2 $w_2(\bar{x}) = 0$, as there is no torsion-bending coupling. The lowest normalized eigenvalue is closely approximated by the limit load $\lambda_s^{nl} = 1.76849$ with $n = 14$ full waves in the circumferential direction (see also the corresponding results in Table 3). Here the buckling mode shape is anti-symmetric with respect to the mid-plane of the shell at $x = L/2$. It is triggered by a small fictitious imperfection

$$\overline{W} = t\bar{\xi}_2 \sin 2\pi\frac{x}{L}\cos 14\frac{y}{R}, \qquad \bar{\xi}_2 = 0.1 \times 10^{-5}. \tag{48}$$

The lowest symmetric buckling mode with $n = 14$ full waves in the circumferential direction is displayed in Fig. 9. The corresponding eigenvalue is closely approximated by the limit load $\lambda_s^{nl} = 1.89035$. The asymmetric part of the symmetric buckling mode is triggered by a small fictitious imperfection

$$\overline{W} = t\bar{\xi}_2 \sin 3\pi\frac{x}{L}\cos 14\frac{y}{R}, \qquad \bar{\xi}_2 = 0.1 \times 10^{-5}. \tag{49}$$

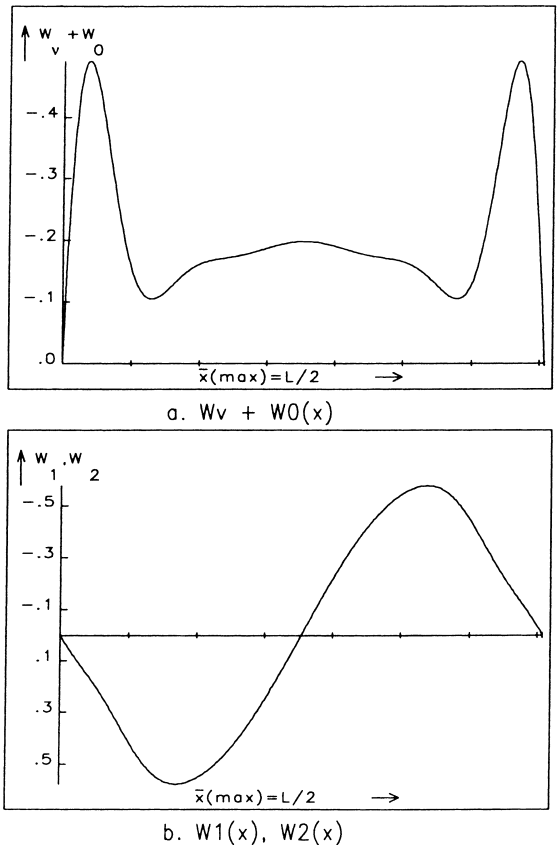

Fig. 8. Critical buckling mode of the axially compressed stringer stiffened shell AS-2 at $\lambda_s^{nl} = 1.76849$ ($n = 14$).

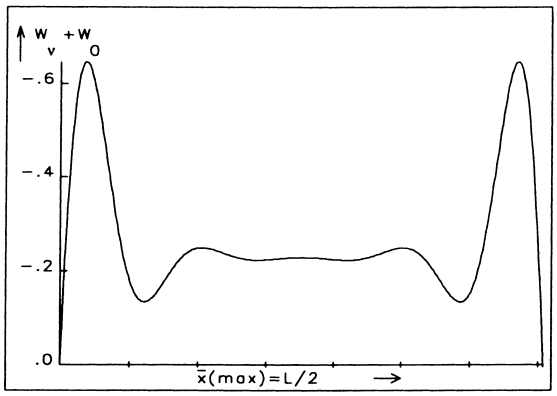

Fig. 9. Lowest symmetric buckling mode of the axially compressed stringer stiffened shell AS-2 at $\lambda_s^{nl} = 1.89035$ ($n = 14$).

4.2. Buckling loads of the imperfect shell

Next, using SS-4 boundary conditions the effect of shape imperfections is investigated, whereby initially the modal imperfection given by Eq. (48) is considered. Koiter (1945, 1967, 1963) has shown that the buckling load of the imperfect shell λ_s (the maximum load the structure can support prior to buckling) is related to the imperfection amplitude $\bar{\xi}_2$ and the second postbuckling coefficient "b" by

$$(1-\rho_s)^{3/2} = (3/2)\sqrt{-3b}\ \rho_s|\bar{\xi}_2|, \quad b<0, \tag{50}$$

where $\rho_s = \lambda_s/\lambda_c^{nl}$. This equation is asymptotically valid for small imperfections. Cohen (1968) and Hutchinson and Frauenthal (1969) have modified this formula to account for the variation between the assumed shape of the modal imperfection and the buckling modes calculated using nonlinear prebuckling analysis and satisfying the specified boundary conditions rigorously. The modified Koiter formula is

$$(1-\rho_s)^{3/2} = (3/2)\sqrt{-3\alpha b}[1-(\alpha/\beta)(1-\rho_s)]\ |\bar{\xi}_2|, \quad b<0, \tag{51}$$

where α and β are the first and second imperfection form factors. Notice that only negative values of the second postbuckling coefficient "b" imply the existence of a limit point and thus a decrease of the load carrying capacity of the imperfect structure. Using ANILISA (Arbocz and Hol, 1990) for the axially

compressed stringer stiffened shell AS-2, one obtains for the close modal approximation of the critical buckling mode given by Eq. (48) the following values:

$$\lambda_c^{nl} = 1.76862\,(n = 14), \quad b = -0.096261, \quad \alpha = 0.74404, \quad \beta = 0.55102. \tag{52}$$

For these values, the results given by Eq. (51) are plotted as the solid curve in Fig. 10.

In order to establish the range of validity of the asymptotic predictions, one must solve the nonlinear 2-point boundary value problem given by Eqs. (40) and (41) for the assumed asymmetric imperfection

$$A_0(x) = 0, \quad A_1(x)\cos n\bar{y} = \bar{\xi}_2 \sin 2\pi \frac{x}{L} \cos 14\bar{y}, \quad A_2(x) = 0. \tag{53}$$

The results obtained are shown as the dotted curve in Fig. 10.

When comparing the two curves shown in Fig. 10, one must remember that Koiter's imperfection sensitivity theory is asymptotically exact, that is, it yields accurate predictions for sufficiently small imperfections, whereby what is sufficiently small may vary from case to case. Further, one must recall that Eqs. (50) and (51) are obtained via perturbation expansions (Cohen, 1968), where terms of $O(\bar{\xi}\bar{\xi})$ are neglected, whereas in the nonlinear computational module COLLAPSE, presented in this article, terms up to order $(\bar{\xi}\bar{\xi}^2)$ are kept. Thus the predictions of COLLAPSE are more accurate, especially for larger values of $\bar{\xi}$.

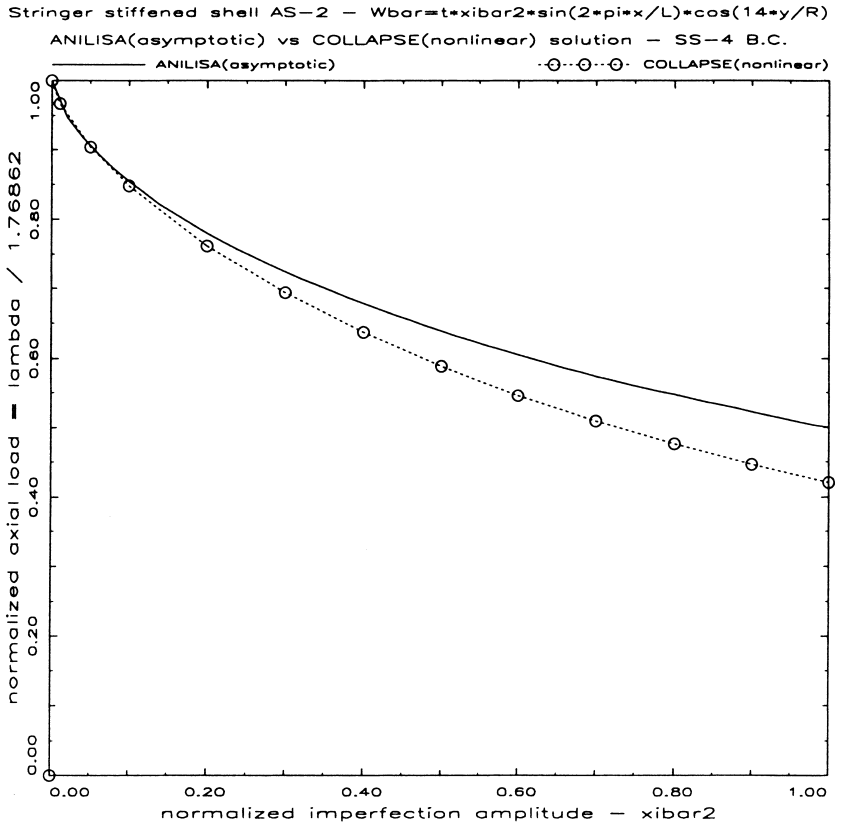

Fig. 10. Imperfection sensitivity of the stringer stiffened shell AS-2 axial compression, nonlinear prebuckling, $u = u_0$, $v = w = M_x = 0$ $\overline{W} = t\bar{\xi}_2 \sin(2\pi x/L)\cos(14y/R)$, $\lambda_c^{nl} = 1.76862$.

A closer look at Fig. 10 reveals that in this case (as expected) the asymptotic predictions are higher, namely at $\overline{\xi}_2 = 0.4$ by about 4%, whereas at $\overline{\xi}_2 = 1.0$ the difference is about 8%.

The shape imperfection considered in Eq. (53) represents the initial deviations of the shell midsurface from the perfect shell configuration and is a close approximation of the critical buckling mode shown in Fig. 8. For comparison purposes, next the effect of the asymmetric imperfection

$$\overline{W} = t\overline{\xi}_2 \sin 3\pi \frac{x}{L} \cos 14 \frac{y}{R} \tag{54}$$

is investigated. Notice that this modal imperfection represents a close approximation of the lowest symmetric buckling mode with $n = 14$ full waves in the circumferential direction shown in Fig. 9. Using ANILISA one obtains the following values

$$\lambda_c^{nl} = 1.89050(n = 14), \quad b = -0.17433, \quad \alpha = 0.74404, \quad \beta = 0.55102. \tag{55}$$

For these values, the results given by Eq. (51) are plotted as the solid curve in Fig. 11. Notice that the normalized axial load, defined as $\lambda/1.76862$, for very small imperfections predicts higher critical loads than the preceding imperfection model. However, for increasing imperfection amplitudes the current imperfection model results in somewhat higher imperfection sensitivity.

To establish the range of validity of the asymptotic predictions next the 2-point nonlinear value problem of Eqs. (40) and (41) is solved using the following asymmetric imperfection

$$A_0(x) = 0, \qquad A_1(x) \cos n\overline{y} = \overline{\xi}_2 \sin 3\pi \frac{x}{L} \cos 14\overline{y}; \qquad A_2(x) = 0. \tag{56}$$

The results obtained are displayed as the dotted curves in Fig. 11. Once again, the asymptotic predictions are somewhat higher than the nonlinear solutions.

4.3. Buckling loads of shells with boundary imperfections

Based on the results of the flatness survey of one of the end-rings used in the test setup of shell AS-2 shown in Fig. 4, let us assume that the flatness variation of the boundary support can be modeled by Eq. (25). To trigger the critical buckling mode of the perfect AS-2 shell with boundary imperfections, initially it is assumed that

$$\text{at } x = 0 \quad u_b = t\overline{u}_{01} \cos 14\overline{y} = t\overline{\xi}_b \cos 14\overline{y}, \tag{57a}$$

$$\text{at } x = L \quad u_b = t\overline{u}_{L1} \cos 14\overline{y} = t\overline{\xi}_b \cos 14\overline{y}. \tag{57b}$$

Notice that these expressions will trigger a response mode W, which is anti-symmetric with respect to the mid-plane of the shell at $x = L/2$, a shape which corresponds to the critical buckling mode of the perfect AS-2 shell with SS-4 boundary conditions shown in Fig. 8. As can be seen from the results plotted in Fig. 12, the anti-symmetric boundary imperfection (where $\overline{u}_{01} = \overline{u}_{L1}$) has a very strong degrading effect on the load carrying capacity of the axially compressed stringer stiffened shell AS-2. A flatness variation of the shape given by Eqs. (57) and an amplitude of one-tenth of the wall thickness ($\overline{\xi}_b = 0.1$, say) reduces the buckling load of the perfect shell by about 60%.

Considering now another possible flatness variation, where at the upper and lower edges the boundary imperfections are out of phase, i.e.

$$\text{at } x = 0 \quad u_b = t\overline{u}_{01} \cos 14\overline{y} = t\overline{\xi}_b \cos 14\overline{y}, \tag{58a}$$

$$\text{at } x = L \quad u_b = -t\overline{u}_{L1} \cos 14\overline{y} = -t\overline{\xi}_b \cos 14\overline{y}, \tag{58b}$$

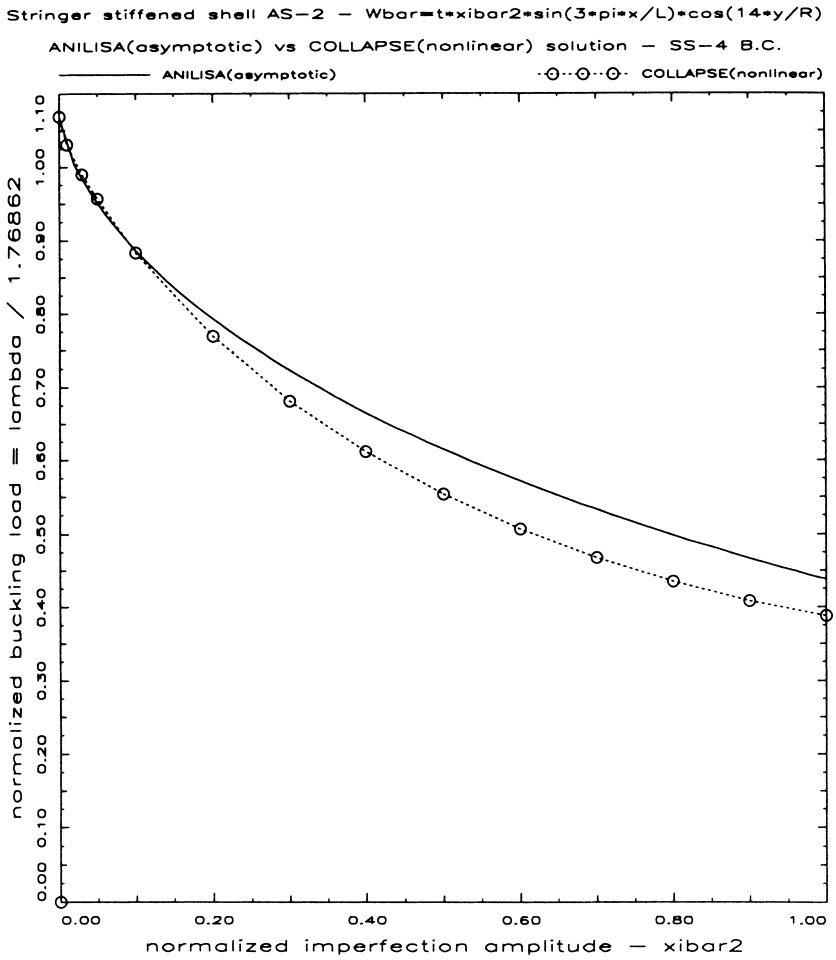

Fig. 11. Imperfection sensitivity of the stringer stiffened shell AS-2 axial compression, nonlinear prebuckling, $u = u_0$, $v = w = M_x = 0$ $\overline{W} = t\overline{\xi}_2 \sin(3\pi x/L)\cos(14y/R)$, $\lambda_c^{nl} = 1.89050$.

then these expressions trigger a response mode W, that is symmetric with respect to the mid-plane of the shell at $x = L/2$. Notice that this mode shape corresponds to the lowest symmetric buckling mode of the perfect AS-2 shell with SS-4 boundary conditions and $n = 14$ full waves in the circumferential direction (see also Fig. 9). As can be seen in Fig. 12, this symmetric boundary imperfection (where $\overline{u}_{01} = -\overline{u}_{L1}$) also has a pronounced degrading effect on the load carrying capacity of the axially compressed stringer stiffened shell AS-2. Notice that as the corresponding perfect shell eigenvalue of $\lambda_c^{nl} = 1.89050$ is rather high, for small enough imperfections ($\overline{\xi}_b < 0.01$, say) the limit loads are higher than the critical buckling load of the perfect AS-2 shell of $\lambda_c^{nl} = 1.76862$. Still, a flatness variation of the shape given by Eqs. (58) and an amplitude of one-tenth of the wall thickness ($\overline{\xi}_b = 0.1$, say) reduces the buckling load of the perfect shell by about 50%.

To verify these predictions, the two cases were rerun with the well-known nonlinear shell analysis code STAGS-A from Almroth et al. (1971a). Thanks to extensive modifications and additions executed by Brogan (1989) of the original source code with the current TU-Delft version of STAGS-A, it is possible to calculate both the limit load and the bifurcation buckling load under very general elastic boundary

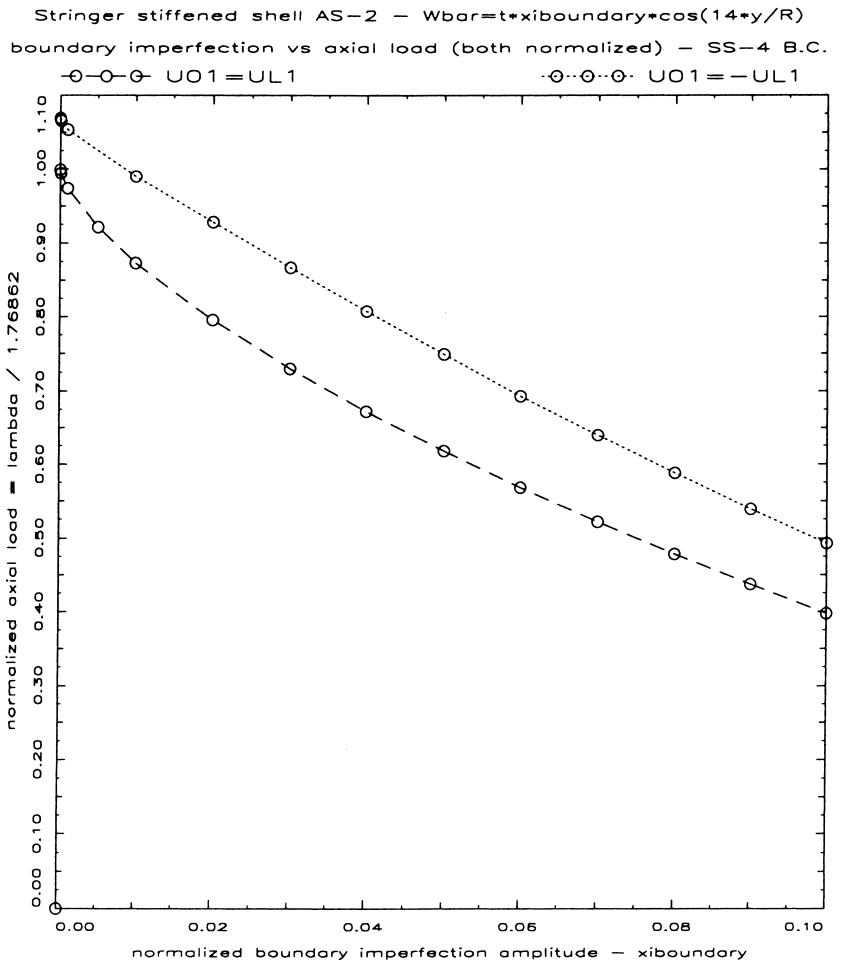

Fig. 12. Imperfection sensitivity of the stringer stiffened shell AS-2 for boundary imperfections $u_b(y) = t\overline{u}_1 \cos 14\overline{y}$, axial compression, $u = u_b$, $v = w = M_x = 0$.

conditions. A comparison of the buckling loads for the anti-symmetric case (where $\overline{u}_{01} = \overline{u}_{L1}$) is shown in Fig. 13. For the symmetric case (where $\overline{u}_{01} = -\overline{u}_{L1}$), the comparison of results is shown in Fig. 14. In both cases, the agreement between the results of COLLAPSE (Donnell type equations) and of STAGS-A (Flügge–Marlowe type equations) is very good. The minor differences seen are due to the different shell equations used.

Notice that in Fig. 14, for the symmetric case (where $\overline{u}_{01} = -\overline{u}_{L1}$) for very small imperfections ($\overline{\xi}_b < 0.01$) with STAGS-A no limit points are found. Also, during the STAGS-A calculations for the symmetric case before reaching the limit point negative roots on the diagonal of the stiffness matrix are detected. This indicates the presence of bifurcation points along the nonlinear prebuckling path. Repeating the calculations, indeed it was found that for symmetric boundary imperfections (where $\overline{u}_{01} = -\overline{u}_{L1}$) close to but before reaching the limit points always bifurcation into a mode occurs, which is antisymmetric with respect to the shell mid-plane at $x = L/2$. However, as can be seen from Fig. 15, for larger imperfections ($\overline{\xi}_b > 0.01$), the agreement between the results obtained by COLLAPSE (limit point calculations) and the STAGS-A bifurcation loads is good.

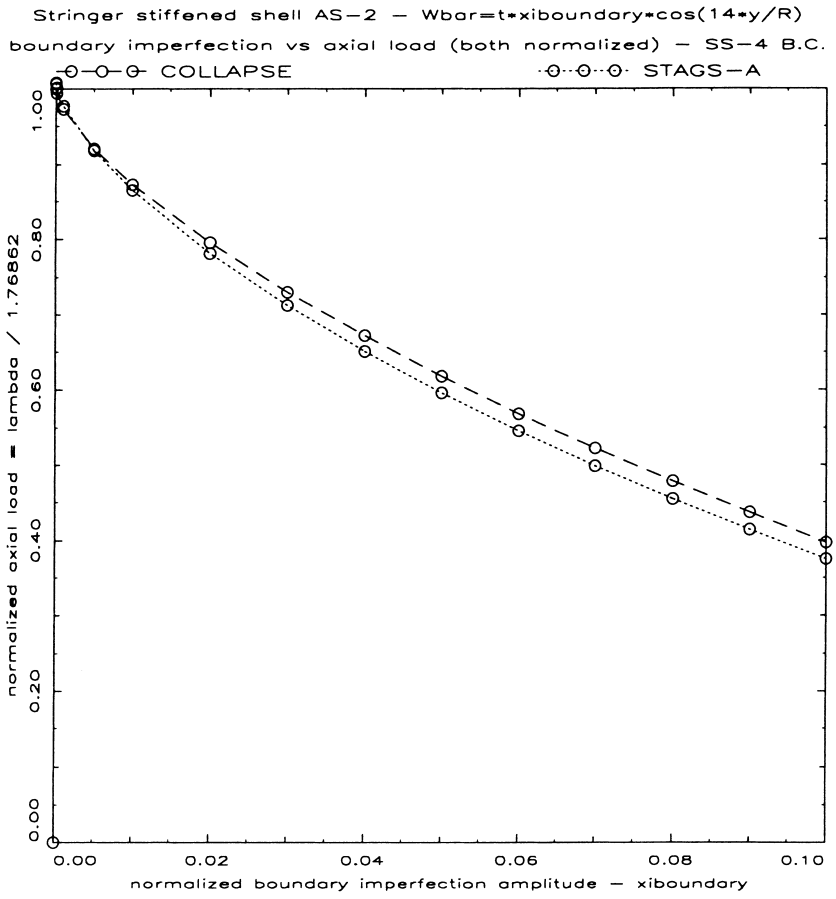

Fig. 13. Comparison of buckling loads for anti-symmetric ($\overline{u}_{01} = \overline{u}_{L1}$) boundary imperfections.

5. Conclusions

Koiter's general theory of elastic stability (1967) has greatly contributed to our understanding of the sometimes perplexing stability behavior of thin-walled structures. With the advent of modern high-speed computers, it became feasible to study those effects, which in Koiter's analytical solutions had to be neglected. The use of nonlinear prebuckling analysis and rigorous satisfaction of the specified boundary conditions (Cohen, 1968; Hutchinson and Frauenthal, 1969; Arbocz and Hol, 1990) have greatly improved the accuracy and the predictive power of Koiter's asymptotic approach.

Using Donnell-type anisotropic shell equations, a rigorous nonlinear solution has been presented for the collapse behavior of imperfect, stiffened, layered composite shells under combined axial compression, internal or external pressure and torsion. These nonlinear solutions make it possible to establish the range of validity of Koiter's asymptotic formula used for the prediction of imperfection sensitivity of the buckling load.

It has been shown that nonuniform, harmonically varying boundary imperfections can have severe degrading effect on the load carrying capacity of axially compressed stringer stiffened shells. It appears that for proper correlation of experimental results and theoretical predictions, at least for stringer stiffened shells, the boundary imperfections must be included in the analysis.

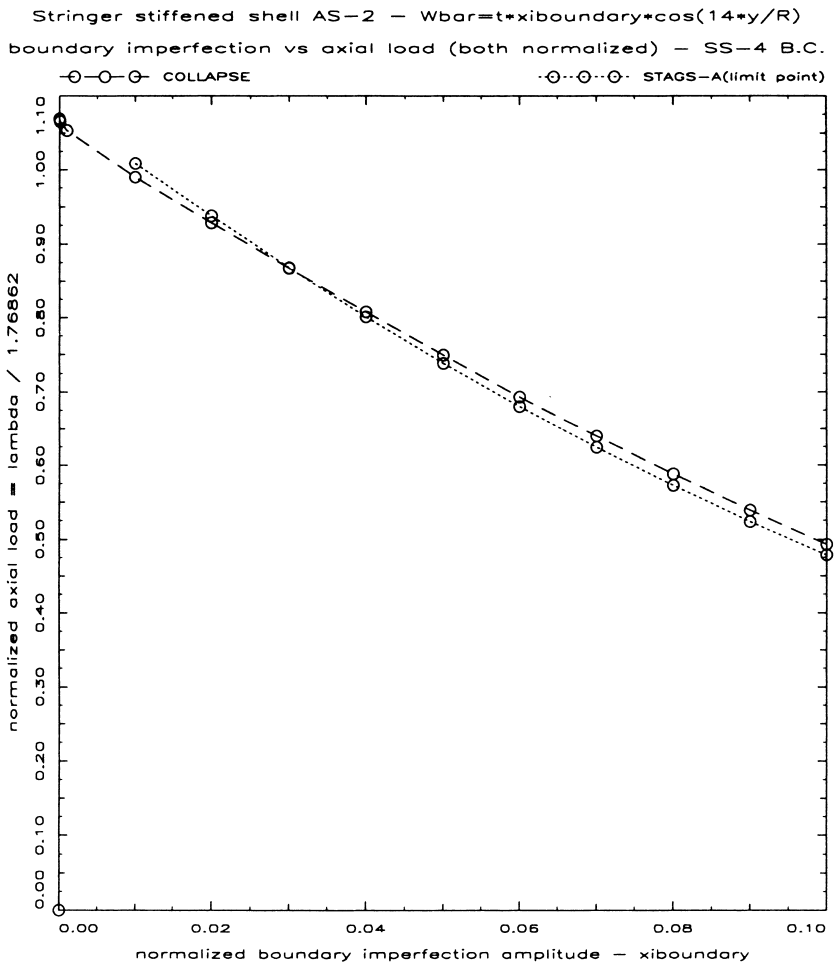

Fig. 14. Comparison of buckling loads for symmetric ($\bar{u}_{01} = -\bar{u}_{L1}$) boundary imperfections.

It must be stressed that the work done with COLLAPSE so far has only demonstrated the importance of accounting for the boundary imperfections, if one wants to achieve an accurate prediction of the load carrying capacity of axially compressed cylindrical shells. It is felt that a systematic investigation of other boundary imperfection models and the effect of nonlinear interaction with shape imperfections must be carried out in order to get a better insight into the buckling behavior of imperfect shells. Especially, the earlier work by Sabag et al. (1989), who solved Flügge's linearized stability equations with membrane prebuckling under nonuniform boundary conditions, should be rerun with the present nonlinear approach. Also, the effect of other external loads such as pressure and torsion must be studied.

Finally, if by a probabilistic prediction of the buckling load one is talking about a probability of failure of 10^{-6}, then the mechanical modeling of the buckling process must be very accurately done. This implies, that in the future the experimentalist must not only measure the shape imperfections, which with modern computer supported laser–theodolite systems (Megson and Hallack, 1992) is now feasible even for very large structures, but he must also provide information about the flatness of the end supports and possibly about the elastic restraint of the rotation of the shell edges, if an accurate prediction of the expected buckling load is required.

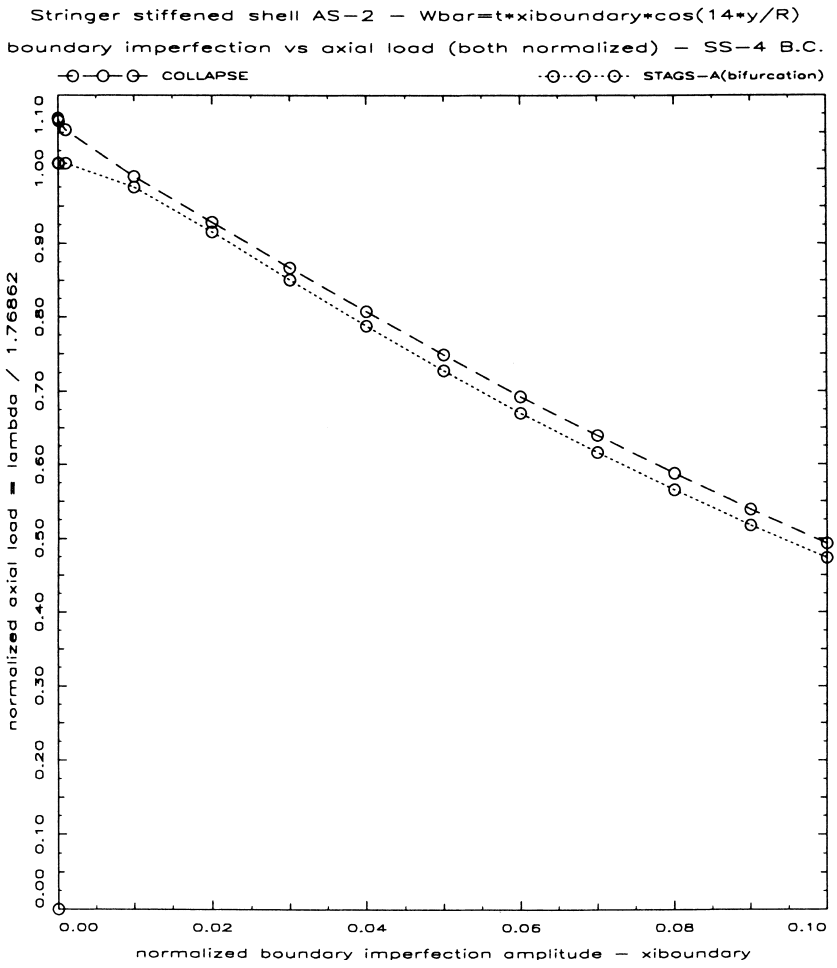

Fig. 15. Comparison of buckling loads for symmetric ($\overline{u}_{01} = -\overline{u}_{L1}$) boundary imperfections (limit loads versus bifurcation loads).

Acknowledgements

This article is dedicated to the memory of Warner Tjardus Koiter, a great scientist who has made many pioneering and seminal contributions to the field of engineering mechanics and especially to elastic stability, a person whom the author had the privilege to have known for over 30 years, first as a graduate student and later as a colleague and friend. The author wishes to thank Mrs. Annemarie van Lienden-Datema for the skillful typing of the manuscript.

Appendix A. Periodicity condition

If the solution is to satisfy the periodicity requirement, then, by definition,

$$\int_0^{2\pi R} v_{,y}\,\mathrm{d}y = 0 \tag{A.1}$$

must hold, where

$$v_{,y} = \varepsilon_y + (1/R)W - (1/2)W_{,y}^{2} - \overline{W}_{,y}\, W_{,y}\,, \tag{A.2}$$

$$\varepsilon_y = A_{12}^{*}N_x + A_{22}^{*}N_y + A_{26}^{*}N_{xy} + B_{21}^{*}\kappa_x + B_{22}^{*}\kappa_y + B_{26}^{*}\kappa_{xy}, \tag{A.3}$$

Further, using the Airy stress function F

$$N_x = F_{,yy}\,, \quad N_y = F_{,xx}\,, \quad N_{xy} = -F_{,xy}\,, \tag{A.4}$$

$$\kappa_x = -W_{,xx}\,, \quad \kappa_y = -W_{,yy}\,, \quad \kappa_{xy} = -2W_{,xy}\,. \tag{A.5}$$

Introducing these expressions into Eq. (A.1) and substituting for $\overline{W}$, W and F from Eqs. (6)–(8), one obtains

$$\begin{aligned}
\int_0^{2\pi} \{ & -\overline{A}_{12}^{*}(\lambda + n^2 f_1 \cos n\overline{y} + 4n^2 f_2 \cos 2n\overline{y} + n^2 f_3 \sin n\overline{y} + 4n^2 f_4 \sin 2n\overline{y}) \\
& + \overline{A}_{22}^{*}(-\overline{p} + f_0'' + f_1'' \cos n\overline{y} + f_2'' \cos 2n\overline{y} + f_3'' \sin n\overline{y} + f_4'' \sin 2n\overline{y}) \\
& - \overline{A}_{26}^{*}(-\overline{\tau} - nf_1' \sin n\overline{y} - 2nf_2' \sin 2n\overline{y} + nf_3' \cos n\overline{y} + 2nf_4' \cos 2n\overline{y}) \\
& - (1/2)(t/R)[\overline{B}_{21}^{*}(w_0'' + w_1'' \cos n\overline{y} + w_2'' \sin n\overline{y}) - \overline{B}_{22}^{*}n^2(w_1 \cos n\overline{y} + w_2 \sin n\overline{y}) \\
& + 2\overline{B}_{26}^{*}n(-w_1' \sin n\overline{y} + w_2' \cos n\overline{y})] + c(W_v + W_p + W_t + w_0 + w_1 \cos n\overline{y} + w_2 \sin n\overline{y}) \\
& - (c/4)(t/R)n^2[w_1(w_1 + 2A_1) + w_2(w_2 + 2A_2) - \langle w_2(w_1 + 2A_1) + w_1(w_2 + 2A_2)\rangle \sin 2n\overline{y} \\
& - \langle w_1(w_1 + 2A_1) - w_2(w_2 + 2A_2)\rangle \cos 2n\overline{y}]\}\mathrm{d}\overline{y} = 0.
\end{aligned} \tag{A.6}$$

Carrying out the $\overline{y}$-integration and introducing the nondimensional quantities defined earlier yields

$$\begin{aligned}
\{ & -\overline{A}_{12}^{*}\lambda - \overline{A}_{22}^{*}\overline{p} + \overline{A}_{22}^{*}f_0'' + \overline{A}_{26}^{*}\overline{\tau} - \overline{B}_{21}^{*}(1/2)(t/R)w_0'' + c(W_v + W_p + W_t) + cw_0 \\
& - (c/4)(t/R)n^2[w_1(w_1 + 2A_1) + w_2(w_2 + 2A_2)]\}(2\pi) = 0.
\end{aligned}$$

Substituting for f_0'' from Eq. (14) and regrouping one obtains

$$(-\overline{A}_{12}^{*}\lambda + cW_v) + (-\overline{A}_{22}^{*}\overline{p} + cW_p) + (\overline{A}_{26}^{*}\overline{\tau} + cW_t) + \tilde{C}_1 x + \tilde{C}_2 = 0.$$

Thus, if

$$W_v = \frac{\overline{A}_{12}^{*}}{c}\lambda, \quad W_p = \frac{\overline{A}_{22}^{*}}{c}\overline{p}, \quad W_t = -\frac{\overline{A}_{26}^{*}}{c}\overline{\tau},$$

$$\tilde{C}_1 = \tilde{C}_2 = 0,$$

then the circumferential periodicity condition is satisfied identically.

References

Almroth, B.O., 1965. Influence of edge conditions on the stability of axially compressed cylindrical shells. NASA CR-161.

Almroth, B.O., Brogan, F.A., Miller, E., Zelle, F., Peterson, H.T., 1971a. Collapse analysis for shells of general shape. Air Force Flight Dynamics Lab., Wright Patterson AFB, AFFDL-TR-71-8.

Almroth, B.O., Brogan, F.A., Marlowe, M.B., 1971b. Collapse analysis of elliptic cones. AIAA Journal 9 (1), 32–37.

Anonymous, 1968. Buckling of thin-walled structures, NASA space vehicle design criteria (structures), NASA SP-8007.

Anonymous, 1988. Buckling of steel shells-European recommendations. ECCS, Technical Working Group 8.4 – stability of shells, ECCS – General Secretariat, Brussels, Belgium.

Arbocz, J., Sechler, E.E., 1973. On the buckling of axially compressed imperfect cylindrical shells. GALCIT SM 73-4, California Institute of Technology, Pasadena, CA.

Arbocz, J., Sechler, E.E., 1974. On the buckling of axially compressed imperfect cylindrical shells. ASME J. Appl. Mech. 41, 737–743.
Arbocz, J., 1975. On the problem of limit point calculation. GALCIT SM 75-7, California Institute of Technology, Pasadena, CA.
Arbocz, J., Sechler, E.E., 1976. On the buckling of stiffened imperfect cylindrical shells. AIAA Journal 14 (11), 1611–1617.
Arbocz, J., 1984. Collapse load calculations for axially compressed imperfect stringer stiffened shells. Proc. 25th AIAA/ASME/ASCE/AHS Structures. Structural Dynamics and Materials Conference. Palm Springs, pp. 130–139.
Arbocz, J., Hol, J.M.A.M., 1989. ANILISA – Computational module for Koiter's imperfection sensitivity theory. Report LR-582, Delft University of Technology, Netherlands.
Arbocz, J., Hol, J.M.A.M., 1990. Koiter's stability theory in a computer aided engineering (CAE) environment. Int. J. Solids Structures 26 (9–10), 945–973.
Arbocz, J., de Vries, J., Hol, J.M.A.M., 1998. On the buckling of imperfect-anisotropic shells with elastic edge supports under combined loading, Part 1: Theory and numerical analysis. Memorandum M-849, Faculty of Aerospace Engineering, Delft University of Technology, Netherlands.
Brogan, F.A., 1989. Personal communication. Delft University of Technology.
Budiansky, B., Hutchinson, J.W., 1964. Dynamic buckling of imperfection sensitive structures. Proc. 11th IUTAM Congress, Springer, Berlin, pp. 636–651.
Budiansky, B., 1965. Dynamic buckling of elastic structures: criteria and estimates. Proc. Int. Conf. Dynamic Stability of Structures. Pergamon Press, Oxford, pp. 83–106.
Cohen, G.A., 1968. Effect of nonlinear prebuckling state on the postbuckling behavior and imperfection sensitivity of elastic structures. AIAA Journal 6 (8), 1616–1619.
Cohen, G.A., 1971. Computer program for analysis of imperfection sensitivity of ring-stiffened shells of revolution. NASA CR-1801.
Hoff, N.J., 1961. Buckling of Thin Shells. Proc. Aerospace Symposium of Distinguished Lectures in Honor of Dr. Theodore von Kármán on his 80th Anniversary, Institute of Aerospace Sciences, New York, pp. 1–42.
Hoff, N.J., Soong, T.C., 1969. Buckling of axially compressed circular cylindrical shells with non-uniform boundary conditions. Proc. Symposium on Thin-walled Structures – their Design and Use in Building. University College of Swansea, pp. 61–80.
Hutchinson, J.W., Amazigo, J.C., 1967. Imperfection sensitivity of eccentrically stiffened cylindrical shells. AIAA Journal 5 (3), 392–401.
Hutchinson, J.W., Frauenthal, J.C., 1969. Elastic postbuckling behavior of stiffened and barreled cylindrical shells. J. Appl. Mech. 36, 784–790.
Keller, H., 1968. Numerical Methods for Two-Point Boundary Value Problems. Blaisdell Publishing Co., Waltham, MA, USA.
Kempner, J., 1954. Postbuckling behavior of axially compressed cylindrical shells. J. Aeronaut. Sci. 21 (5), 329.
Koiter, W.T., 1945, 1967. On the stability of elastic equilibrium. Ph.D. Thesis in Dutch, TH-Delft, Netherlands, H.T. Paris, Amsterdam (English translation issued as NASA TTF-10, p. 833).
Koiter, W.T., 1963. The effect of axisymmetric imperfections on the buckling of cylindrical shells under axial compression. Proc. Koninkl. Nederl. Akademie van Wetenschappen, vol. 66, ser. B, pp. 265–279.
Megson, T.H.G., Hallack, G., 1992. Measurement of the Geometric Initial Imperfections in Diaphragms. Thin-walled Structures, vol. 14, pp. 381–394.
Ohira, H., 1961. Local buckling theory of axially compressed cylindrical shells. Proc. 11th Japan National Congress of Applied Mechanics. pp. 37–40.
Sabag, M., Stavsky, Y., Greenberg, J.B., 1989. Buckling of edge damaged, cylindrical composite shells. ASME J. Appl. Mech. 56, 121–126.
Singer, J., Arbocz, J., Babcock, C.D., 1971. Buckling of imperfect stiffened cylinders under axial compression. AIAA Journal 9 (1), 68–75.
Singer, J., 1979. Recent studies on the correlation between vibration and buckling of stiffened cylindrical shells. Zeitschrift für Flugwissenschaften und Weltraumforschung 3, 333–344.
Singer, J., 1983. Vibrations and buckling of imperfect stiffened shells – recent developments. Proc. IUTAM Symposium: Collapse, the buckling of structures in theory and practice. In: Thompson, J.M.T., Hunt, G.W. (Eds.), Cambridge University Press, Cambridge, pp. 443–479.
Tennyson, R.C., Muggeridge, D.B., 1969. Buckling of axisymmetric imperfect circular cylindrical shells under axial compression. AIAA Journal 7 (11), 2127–2131.
Weller, T., Singer, J., 1971. Experimental studies on the buckling of 7075-T6 aluminum alloy integrally stringer stiffened shells, TAE Report no. 135, Technion Research and Development Foundation, Haifa, Israel.